




A Method for Estimating the Rheological Properties of Fractured Rock Inside a Shear Zone

ZUAN CHEN,^{1,2}  XIAN LI,^{2,3} XIAOGE HUANG,² and ZHIHE JIN⁴

Abstract—This paper is concerned with the creep properties of fractured rock in a shear zone. We consider a cube rock model which consists of the rock matrix and cracks. A finite element method with discontinuous deformation analysis (DDA) is used to simulate the creep response of the fractured rock sample. The DDA is used to describe the interactions among the contacting blocks at their interfaces (cracks). In all numerical simulations of the creep test, the strain rates are those typical values corresponding to effective viscosities of 10^{17} – 10^{19} Pa s, similar to that obtained from geophysical observations in a shear zone. The effects of temperature, confining pressure, crack length and tilt on the creep responses are examined using the simulation results. The numerical results indicate that our method is a useful tool for simulating creep deformation of fractured rock. The present study represents an effort to use a numerical method to simulate the rheological properties of fractured rock in the field of micro-geodynamics.

Keywords: Fractured rock, rheological properties, numerical simulation, shear zone.

1. Introduction

In the last decade, a new geophysical theory has been proposed. It is assumed in the theory that closely spaced stress-aligned microcracks pervade the crust and uppermost ~ 400 km of the mantle of the Earth; in situ rocks are close to failure by fracturing; a series of shear zones with low viscosity are formed, and hence they produce critical systems that possess new properties on conventional subcritical geophysics

(Crampin, 2011, 2012; Crampin & Gao, 2018; Jordan & Jones, 2011). These new properties have confirmed that the new geophysical theory is a novel understanding of fluid/rock deformation with important implications and applications, for example, causing the formation of seismic anisotropy, as an explanation for earthquake behavior and oceanic spreading, and so on.

The rheological properties of perfect rock and mineral crystals under mantle conditions have been widely studied using both experimental and theoretical methods. Applications of the new geophysical theory require knowledge of the rheological properties of fractured rocks after strain localization, which are still not well understood. Grain boundary sliding (GBS) has recently been identified as an important deformation mechanism during creep of rock aggregation (Hansen et al., 2011; Hirth & Kohlstedt, 1995; Karato et al., 1986). Extensive experimental work has been conducted on the GBS of rock, and a GBS flow law has been presented through these experiments (Hirth & Kohlstedt, 2003). It indicates that GBS is a dominant deformation mechanism at high stresses and low temperatures under which fine-grained shear zones are often observed (Warren & Hirth, 2006). GBS is also considered to be a major cause of strain localization in the Earth's lithosphere and a mechanism for weakening of the subcontinental mantle (Précigout et al., 2007).

Several physical mechanisms may be responsible for GBS, for example, dislocation motion and diffusion. When the deformation of rock is localized inside a shear zone, sliding and rotation on the grain boundary during creep deformation will be a dominant deformation mechanism. This work is concerned with numerical simulation of the rheological properties of fractured rock inside a shear zone. We first briefly introduce our proposed numerical method. We

¹ Key Laboratory of Shale Gas and Geoengineering, Institute of Geology and Geophysics, Chinese Academy of Sciences, Beijing 100029, China. E-mail: zachen@mail.iggcas.ac.cn

² Key Laboratory of Earth and Planetary Physics, Institute of Geology and Geophysics, Chinese Academy of Sciences, Beijing 100029, China.

³ University of Chinese Academy of Sciences, Beijing 100049, China.

⁴ Department of Mechanical Engineering, University of Maine, Orono, ME 04469, USA.

then apply the numerical technique to simulate creep response using a physical model to estimate the rheological properties of fractured rock. Finally, we discuss the numerical results and the validity of our numerical method, and provide conclusions.

2. The Numerical Method

Grain boundary sliding and rotation involve interactions among all of the grains in contact. At the end of the previous century, considerable effort was invested in understanding contact problems with friction (Peric & Owen, 1992). Ghahremani (1980) presented a numerical method to deal with GBS. In this paper, we present a different numerical technique to simulate GBS. We have developed a three-dimensional discontinuous deformation analysis–finite element method (3D DDA+FEM) program under some simplified assumptions based on previous research (Chen et al., 2011). The DDA is used to deal with the interactions among contacting blocks at their interfaces, and FEM is used to determine the deformation inside the blocks, as schematically shown in Fig. 1. In this work, the 3D DDA+FEM program (Chen et al., 2011) has been upgraded so that it can be used to simulate GBS of rock aggregation and analyze its effect during creep deformation. In our program, it is assumed that the displacement is small and the points of contact among the grains are known. The constitutive behavior of the contact surfaces between the blocks is described by springs and viscous dampers in series as shown in Fig. 1a. A brief introduction of the computational method is described as follows.

We assume that the rock consists of many grains and that each grain is divided into some finite elements as shown in Fig. 1. We use isoparametric hexahedron elements with eight nodes in the numerical program because accurate results can be obtained with the element. The isoparametric elements also can be adapted to the geometries of rock

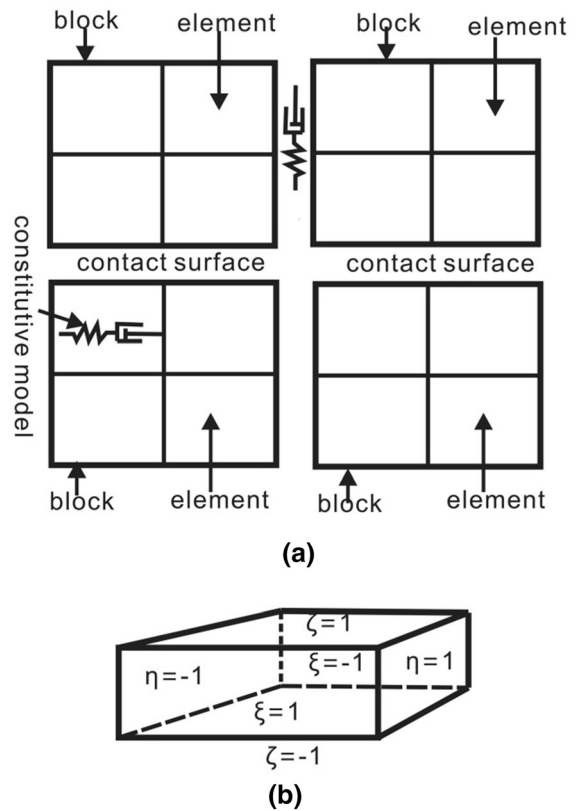


Figure 1

a A schematic of the elements and the interface in the numerical method, **b** the local coordinates of the six surfaces of a hexahedron element ($\xi = \pm 1$, $\eta = \pm 1$, and $\zeta = \pm 1$)

samples. The nodal coordinates are denoted by \mathbf{x}_i (x_i , y_i and z_i) ($i = 1, 2, \dots, 8$), and the nodal displacements are \mathbf{u}_i (u_i , v_i and w_i) ($i = 1, 2, \dots, 8$). Their shape functions are denoted by N_i (ξ, η, ζ) ($i = 1, 2, \dots, 8$), where ξ, η , and ζ are the local coordinates with the element surfaces described by $\xi = \pm 1$, $\eta = \pm 1$, and $\zeta = \pm 1$ as shown in Fig. 1b. The shape functions for the 8-node isoparametric element are given by

$$N_i = \frac{1}{8}(1 + \xi_i \xi)(1 + \eta_i \eta)(1 + \zeta_i \zeta) \quad (1)$$

$$(-1 \leq \xi, \eta, \zeta \leq 1; \xi_i, \eta_i, \zeta_i = \pm 1)$$

The displacement within the element is

$$\mathbf{u} = \begin{bmatrix} u \\ v \\ w \end{bmatrix}$$

$$= [IN_1 \ IN_2 \ IN_3 \ IN_4 \ IN_5 \ IN_6 \ IN_7 \ IN_8]$$

$$\begin{bmatrix} \mathbf{u}_1 \\ \mathbf{u}_2 \\ \mathbf{u}_3 \\ \mathbf{u}_4 \\ \mathbf{u}_5 \\ \mathbf{u}_6 \\ \mathbf{u}_7 \\ \mathbf{u}_8 \end{bmatrix} = \mathbf{N}a^e \tag{2}$$

where I is a 3×3 unit matrix, \mathbf{N} is a 3×24 matrix which consists of N_i ($i = 1,2...8$) and a^e is a 24×1 matrix which consists of \mathbf{u}_i ($i = 1,2...8$). The relationship between the strain and nodal displacements of the element is

$$\varepsilon = [B_1 \ B_2 \ B_3 \ B_4 \ B_5 \ B_6 \ B_7 \ B_8]a^e = \mathbf{B}a^e \tag{3}$$

where \mathbf{B} is the strain matrix. The stress in the element undergoing elastic deformation is given by the generalized Hooke's law:

$$\sigma = D\varepsilon = \mathbf{D}\mathbf{B}a^e \tag{4}$$

where \mathbf{D} is the elasticity matrix containing the specific material properties.

The total potential energy in the minimum potential energy principle is

$$\Pi_u = \int_V \frac{1}{2} \varepsilon^T D \varepsilon dx dy dz - \int_V u^T f dx dy dz - \int_{S_\sigma} u^T T dS \tag{5}$$

where \mathbf{f} is the body force, \mathbf{T} is the traction, V is the volume and S_σ is part of the boundary on which the traction is applied.

For the finite element model, the potential energy of the system is the sum of the potential energies of all elements, i.e.,

$$\begin{aligned} \Pi_u &= \sum_e \Pi_u^e = \sum_e \left(a^{eT} \int_{V_e} \frac{1}{2} \mathbf{B}^T \mathbf{D} \mathbf{B} dx dy dz a^e \right) \\ &\quad - \sum_e \left(a^{eT} \int_{V_e} \mathbf{N}^T \mathbf{f} dx dy dz \right) - \sum_e \left(a^{eT} \int_{S_\sigma^e} \mathbf{N}^T \mathbf{T} dS \right) \end{aligned} \tag{6}$$

We assume that point P on the surface of block A is in contact with point Q of block B, as shown in Fig. 2. The coordinates and displacements of the contact points are respectively denoted by \mathbf{x}_P , \mathbf{u}_P , \mathbf{x}_Q and \mathbf{u}_Q . The relationship between the coordinates and displacements of $\mathbf{x}_{Q/P}$ and $\mathbf{u}_{Q/P}$ and the eight nodes of the finite element to which point Q/P belongs is as follows:

$$x_{Q/P} = \sum_{i=1}^8 N_i(\xi_{Q/P}, \eta_{Q/P}, \zeta_{Q/P}) x_i \tag{7}$$

$$u_{Q/P} = \sum_{i=1}^8 N_i(\xi_{Q/P}, \eta_{Q/P}, \zeta_{Q/P}) u_i \tag{8}$$

The displacement of points P and Q in the local coordinates on the contact surface are expressed by u^A and u^B , respectively.

The total strains on the contact surface contain two parts

$$\varepsilon_f = \frac{u^A - u^B}{w} = \frac{u_e^A - u_e^B}{w} + \frac{u_c^A - u_c^B}{w} = \frac{u_e^A - u_e^B}{w} + \varepsilon_f^c \tag{9}$$

where subscript e represents elasticity, and superscript c represents creep. In Eq. (9), w is a length parameter between the two contact surfaces.

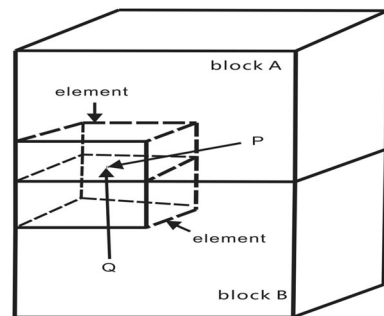


Figure 2
A schematic of the elements and contact points on the interface

When the two blocks are bonded at the contact points, the contact stresses are related to the separation displacements by the following spring relations for the normal and tangential components:

$$\sigma_n^f = \lambda_1 \left(\frac{u_n^A - u_n^B}{w} \right), \quad \sigma_t^f = \lambda_2 \left(\frac{u_{te}^A - u_{te}^B}{w} \right) \quad (10)$$

where λ_1 and λ_2 are a type of virtual spring constants that are generally taken to be very large so that penetration between the contact points is prevented. We note that λ_1 and λ_2 are not the traditional spring constants but have the unit of stress. In Eq. (10), subscript n and t represent the normal and tangential components on the contact surface.

For the creep problem, the total strain is the sum of the elastic strain and the creep strain

$$\varepsilon = \varepsilon^e + \varepsilon^c \quad (11)$$

The stress in an element is related to total and creep strains as follows:

$$\sigma = D(\varepsilon - \varepsilon^c), \quad \Delta\sigma = D(\Delta\varepsilon - \Delta\varepsilon^c) \quad (12)$$

where Δ represents the increment.

Inside the block (i.e., the grain), the creep strain follows a power law (Karato, 2008), i.e.,

$$\Delta\varepsilon^c = A\sigma^n \exp\left(-\frac{E + PV}{RT}\right)\Delta t, \quad (13)$$

where A is a pre-exponential material constant, n is the power law creep index, E is the activation energy, V is the activation volume, R is the universal gas constant. σ , P and T are, respectively, the differential stress, pressure and temperature. The material parameters in Eq. (13) can be determined by rheological tests on mineral under high temperatures and high pressures (Karato, 2008).

On the boundary of the block (grain), we assume that only relative sliding deformation occurs, i.e., the normal strain is zero and the tangential strain follows the relation

$$\varepsilon_{fn}^c = 0; \quad \varepsilon_{ft}^c = \frac{\sigma_t^f}{\eta}\Delta t \quad (14)$$

where η describes the viscosity for the contact surface, and friction between the contact surfaces is neglected.

Then total potential energy is now expressed as

$$\begin{aligned} \Pi_u &= \int_V (\sigma + \Delta\sigma) \cdot \varepsilon dx dy dz \\ &\quad - \int_V u^T f dx dy dz - \int_{S_c} u^T T dS \end{aligned} \quad (15)$$

With regard to contact, we will use the penalty function algorithm to introduce additional constraint conditions into the function to find the solution. Therefore, the potential energy functional is expressed as follows:

$$\Pi = \Pi_u + \Pi_{CP} \quad (16)$$

where Π_{CP} is the additional functional of the definite solution condition that was introduced using the penalty function (Zienkiwicz et al., 2005). The penalty function method belongs to a kind of generalized variational method. For surfaces in contact, this functional is given by (Zienkiwicz et al., 2005)

$$\begin{aligned} \Pi_{CP} &= \int_{S_c} \frac{1}{2w} [\lambda_1 (u_n^A - u_n^B)^2 + \lambda_2 (u_{1e}^A - u_{1e}^B)^2 \\ &\quad + \lambda_2 (u_{2e}^A - u_{2e}^B)^2] dS \end{aligned} \quad (17)$$

where S_c is the contact surface, $\frac{\lambda_i}{w}$ ($i = 1, 2$) are two penalty numbers and λ_i , w have physical meanings as shown in Eqs. (9) and (10). The larger the value of $\frac{\lambda_i}{w}$ ($i = 1, 2$), the better the constraints that will be achieved. The equation for the solution of the finite element of the penalty function algorithm is

$$({}^tK_L + K_{ca})u = {}^{t+\Delta t}Q_c + {}^{t+\Delta t}Q_{fc} - {}^tF \quad (18)$$

where tK_L is the stiffness matrix of the ordinary finite element, K_{ca} is the contribution of the contact surface to the stiffness matrix,

$$\begin{aligned} {}^{t+\Delta t}Q_c &= \sum_e \int_{ve} B^T D \Delta\varepsilon^c dV \\ {}^{t+\Delta t}Q_{fc} &= \sum_{se} \int_{se} N^T \lambda \Delta\varepsilon_f^c dS \\ {}^tF &= - \sum_e \left(\int_e N^T f dV + \int_{S_{se}} N^T T dS \right) \\ &\quad + \sum_e \int_{Ve} B^T \sigma dV \end{aligned} \quad (19)$$

${}^{t+\Delta t}Q_c$ is the additional load caused by creep inside the grains, ${}^{t+\Delta t}Q_{fc}$ is the additional load caused by the

slippage of the contact surface, and F is the equivalent nodal force of the ordinary additional load. Equation (18) can be solved by an iteration method.

3. The Model of Fractured Rock and Numerical Simulation of Its Creep Process

This paper is concerned with the rheological properties of fractured rock in a shear zone after strain localization. In the numerical simulation, we consider a cuboid rock model which contains nine parallel oblique cracks and the two crack faces are in close contact as shown in Fig. 3. The fractured rock sample has dimensions of 4 cm x 8 cm x 8 cm which are typical in experimental creep tests. The model contains 640 elements with 935 nodes. A uniformly distributed load is applied on the six surfaces of the model to simulate a triaxial laboratory creep test. We consider several loading cases in which the confining pressure is 300 MPa along the x -axis and y -axis; differential stresses are 50, 100 and 150 MPa, and temperatures are 1073, 1173 and 1373 K, respectively. The rheological constitutive relation inside the grains is assumed as follows:

$$\dot{\epsilon}^c = A_g \sigma^{n_g} \frac{1}{d^m} \exp\left(-\frac{E_g + V_g P}{RT}\right) \quad (20)$$

In the numerical simulations, our conditions of pressure and temperature are similar to those used in the experimental study of Hansen et al. (2011) on olivine. According to the experimental analysis of Hansen et al. (2011), diffusion is responsible for the creep deformation in the olivine grains. The parameters in Eq. (20) are thus selected as follows:

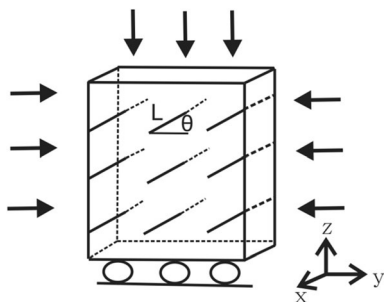


Figure 3
Schematic illustration of model

$$A_g = 10^{7.6} \mu\text{m}^3 / (\text{MPa}^{1.1} \text{s}); \quad d = 30 \mu\text{m}; \quad m = 3; \\ E_g = 375 \text{ kJ mol}^{-1}; \quad V_g = 0; \quad n_g = 1.1.$$

Our simulations using the above parameters produce a viscosity on the order of 10^{20} – 10^{24} Pa s inside the grains.

Consistent with Eq. (14), the rheological constitutive relation on the crack surface is assumed as follows:

$$\dot{\epsilon}_f^c = \sigma_t / \eta \quad (21)$$

where the material parameter is selected as follows: $\eta/w = 10^{14}$ MPa s/cm

η describes the viscosity of the contact surface. In general, the tangential creep strain rate may be a nonlinear function of the tangential contact stress. Here we assume a linear relation for numerical convenience that can also capture the creep behavior of the contact surface. Here we are mainly concerned with sliding between the two contacting surfaces, and thus the normal stress is neglected in the relationship in Eq. (21).

We can see from Eq. (21) that the time increment is confined by η/w in the calculation. Because of lack of experimental data, we chose η/w using multiple numerical tests.

Figure 4 shows all creep curves calculated from the numerical model under various temperature and pressure conditions. The two penalty numbers λ_i/w ($i = 1, 2$) are taken as 10^7 MPa/cm. The time step is selected as 3.6×10^8 s, which guarantees that stresses are constant during the creep process. We found in the numerical simulations that time steps larger than 3.6×10^8 s resulted in decreasing stresses with time, which is not a creep process we studied (we study creep under constant stresses). The strains in these figures represent the average strain of the whole sample. The axial strain is along the direction of the maximum principle stress (z -axis direction). The creep deformation is steady (constant creep strain rate). Table 1 lists the strain rate during the steady creep process under all loading and temperature conditions.

We consider the case in which the crack length is 2.828 cm and crack direction is 45° . We will perform a parametric study on the effects of crack length and orientation in Sect. 4.6. The constitutive relation of the fractured rock is thus assumed as

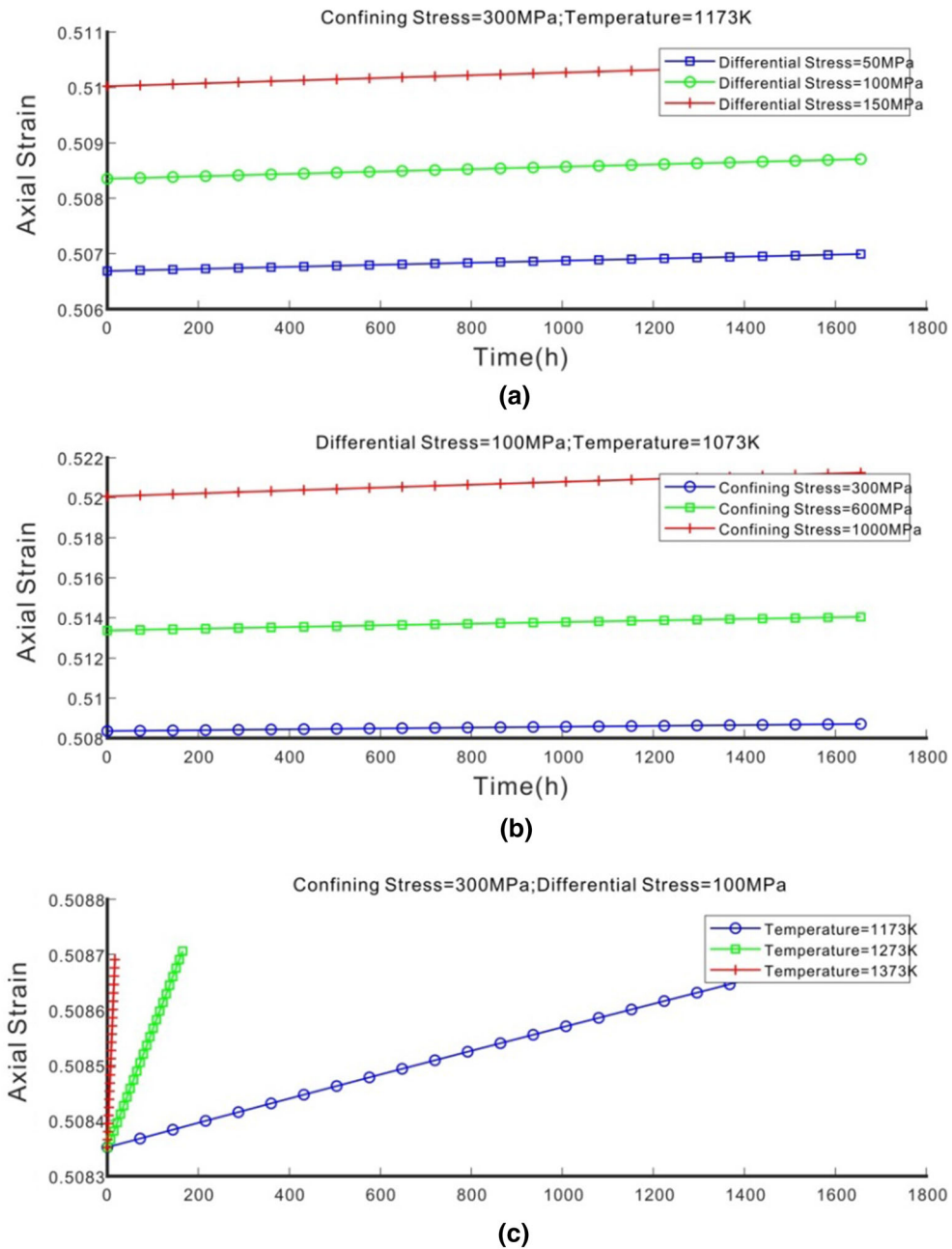


Figure 4 Creep curves of numerical tests under various conditions of pressure and temperature (a, b, c)

$$\dot{\epsilon} = A_0 \sigma^{n_f} \exp\left(-\frac{E_f + pV_f}{RT}\right) \quad (22)$$

The parameters in the above constitutive relation (22) can be determined by the numerical results. We obtain that $A_0 = 5.3128 \times 10^{-11} \text{ MPa}^{-0.26}/\text{s}$,

$E_f = 6.687 \text{ kJ mol}^{-1}$, $V_f = -17.0 \text{ cm}^3 \text{ mol}^{-1}$, and $n_f = 0.26$. These parameters are for the fractured rock and can be different from those in Eq. (20) for the grain.

Figure 5a shows the relationship between the strain rate and differential stress. According to the

Table 1

The results of strain rate obtained from the numerical model at different pressures and temperatures

Confining pressure (MPa)	Differential stress (MPa)	Temperature (K)	Crack length (cm) Crack direction	Strain rate (/s)
300	100	1073	2.828, 45°	1.1512×10^{-10}
300	100	1173	2.828,45°	1.1688×10^{-10}
300	100	1273	2.828,45°	1.1931×10^{-9}
600	100	1073	2.828,45°	2.1775×10^{-10}
1000	100	1073	2.828,45°	3.8361×10^{-10}
300	50	1173	2.828,45°	1.095×10^{-10}
300	150	1173	2.828,45°	1.3246×10^{-10}

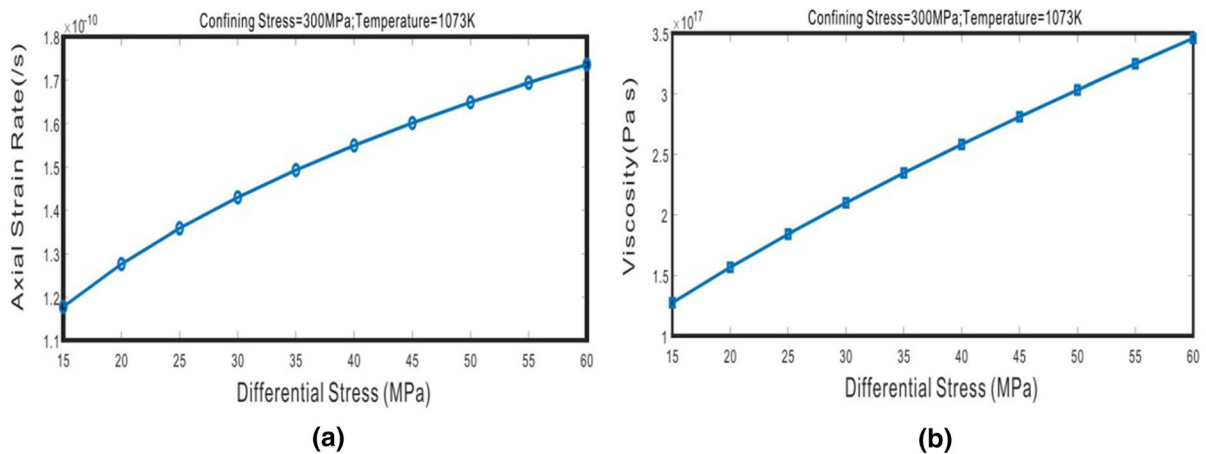


Figure 5

a Relationship between strain rate and differential stress under confining pressure = 300 MPa and temperature = 1073 K; **b** Relationship between viscosity and differential stress under confining pressure = 300 MPa and temperature = 1073 K

equation on the effective viscosity $\eta = \sigma/\dot{\epsilon}$, we obtain the effective viscosity as a function of the differential stress as shown in Fig. 5b. The order of the calculated viscosity is in agreement with the geophysical observation in a fracture zone (Craig & Mckenzie, 1986).

4. Discussion

We have carried out numerical calculations to simulate creep test of fractured rock in a shear zone using the 3D DDA+FEM technique described in Sect. 2. The strain rates are similar in all cases

corresponding to viscosities of 10^{17} – 10^{19} Pa s, in accord with geophysical observation in a fracture zone (Warren & Hirth, 2006). Our numerical result of the effective viscosity (blue line) at a total strain rate of 10^{-10} – 10^{-11} s⁻¹ is in agreement with the geophysical observations. Some special characteristics can be found from the numerical results as follows.

4.1. Temperature Effect

Our numerical results reveal that temperature has the same effect on strain rate and viscosity as diffusion creep of rock grains. Temperature has little effect on crack surface sliding without diffusion or

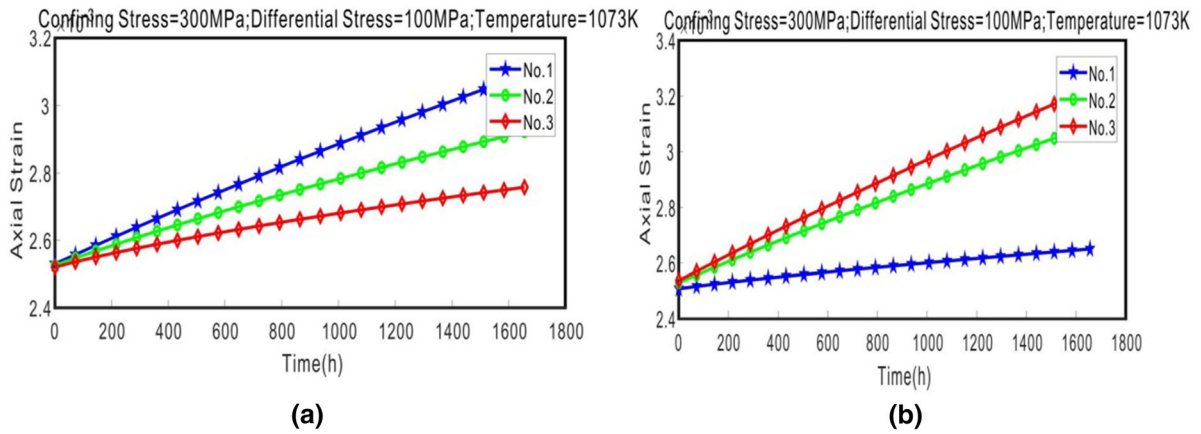


Figure 6

a The tilt is 45° in all three cases; the crack lengths are 2.828 cm for No. 1, 2.121 cm for No. 2 and 1.414 cm for No. 3, respectively. **b** The crack length in three cases is 2.121 cm; the tilts are 75° for No. 1, 45° for No. 2 and 35° for No. 3, respectively

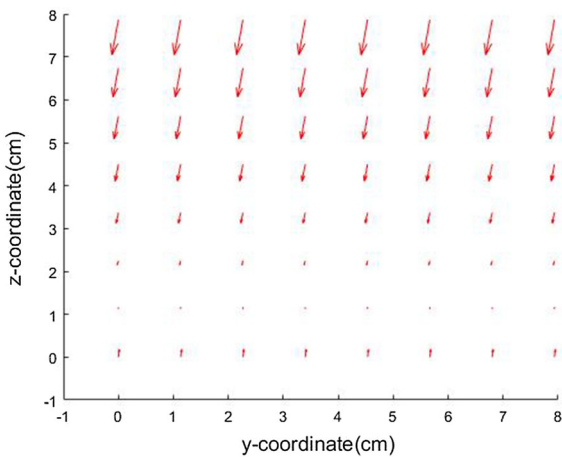


Figure 7

The displacement field map on y-z plane

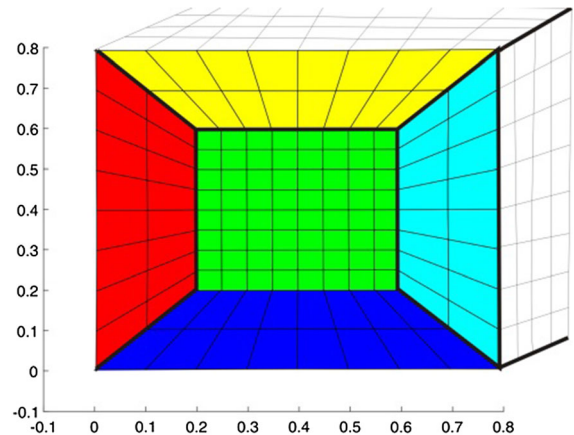


Figure 8

A second model of fractured rock sample and finite element meshing and five quadrangle grains are divided by eight boundary plans (black lines) which simulate cracks in the fractured rock

dislocation in our model. Also, the activation energy E is much smaller than that for perfect defect-free rock. The rheology of sliding cracks leads to an effective rheological law similar to the one corresponding to grain creep.

4.2. Differential Stress Effect

The differential stress does not change the order of magnitude for the strain rate or viscosity. The

strain rate obtained from our numerical calculations is on the order of 10^{-10} /s– 10^{-11} /s, which corresponds to the value in the shear zone. The viscosity is on the order of 10^{17} – 10^{19} Pa s. It is seen from Fig. 4 that both the strain rate and viscosity increase with increasing differential stress. This is probably because the normal force on the crack surface increases with increasing differential stress. As a result, the viscosity of fractured rock is increased.

4.3. Confining Pressure Effect

Our numerical results indicate that higher confining pressure causes larger strain. This is because our model is not isotropic in geometric structure, and higher confining pressure produces larger deformation. We will use more complex rock models to obtain more accurate results in a future study.

4.4. Selection of Viscosity for Crack Surface Sliding

Numerous numerical tests have shown that it is suitable for the viscosity describing crack surface creep sliding (η/w) to be taken as 10^{20} Pa s or greater. Numerical simulations may become unstable if the order of η/w is smaller than 10^{20} Pa s. From Eq. (21), we can see that if η/w is taken to be smaller than 10^{20} Pa s, the time step also needs to be reduced.

From our calculations, we find that the creep strain rate in the fractured rock sample increases with a decrease in the rheological parameter η for the tangential strain rate between the crack surfaces. For the case of a liquid-filled crack, the parameter η will become smaller due to the presence of the liquid phase. Thus, the viscosity of the fractured rock will also become smaller.

4.5. Effect of Crack Length and Direction

In order to examine the effect of crack density and direction, we carry out two group simulations as shown in Fig. 6: (1) different crack lengths with the same orientation; (2) different orientations with the same crack length. The results show that under the same conditions of stress, temperature and tilt, the longer the crack, the larger the strain rate. This is in agreement with our knowledge (Yang et al., 2004). The strain rate is $1.08 \times 10^{-10}/s$, $8.8 \times 10^{-11}/s$, and $2.1 \times 10^{-11}/s$, when the tilt is 35° , 45° , 75° , respectively: the larger the tilt, the smaller the strain rate.

4.6. Displacement Field Inside the Sample

Figure 7 shows the displacement field on the y - z plane in the sample during the creep deformation process. It is seen that the displacement direction

experiences larger variations due to the existence of cracks, which is in agreement with our experience.

4.7. Influence of Initial Crack Model

Two species of microcracks in the crust and in the subcritical system were introduced by Crampin and Gao (2014). One is the closely spaced stress-aligned microcracks as shown as Fig. 3 in this paper, and the other is stress-aligned vertical fluid-saturated microcracks which pervade almost all rocks throughout the Earth's upper crust, lower crust, and uppermost ~ 400 km of the mantle. We construct a second model of fractured rock as shown in Fig. 8, and carry out numerical calculation under the same conditions of temperature and pressure as in Fig. 3. The results indicate that the strain rates are similar, corresponding to viscosities of 10^{17} – 10^{19} Pa s, values in good agreement with geophysical observation in a fracture zone (Warren & Hirth, 2006). But the size of grain influences the value of creep strain rate. The larger the grain size, the smaller the creep strain rate. For the elastic properties, the axial strain of the sample shown in Fig. 3 is larger than that of the sample shown in Fig. 8.

5. Conclusion

In this paper, we simulate the rheological properties of fractured rock inside a shear zone using a 3D FEM+DDA model. Creep curves under various temperature and pressure conditions are obtained using a cuboid rock model which contains nine parallel oblique cracks, and the two crack faces are in close contact. In all the numerical simulations of the creep test, the strain rates are similar, corresponding to viscosities of 10^{17} – 10^{19} Pa s, values in good agreement with geophysical observation in a fracture zone. Moreover, our numerical results show that (i) temperature has less effect on strain rate or viscosity, (ii) the differential stress does not change the order of magnitude for the strain rate or viscosity, and (iii) higher confining pressure causes larger strain. Moreover, longer cracks lead to larger strain rates, and larger crack tilts lead to lower strain rates. The

numerical results indicate that our method is a useful tool to simulate creep deformation of fractured rock. The evolution of the stress field inside the sample also supports this conclusion. The present study represents an effort to use a numerical method to study the rheological properties of fractured rock in the field of micro-geodynamics. We will develop more complex rock models to further study the effectiveness of our numerical method.

Acknowledgements

This research was supported by Yunnan Major Science and Technology Special Project (202002AF080003), the National Natural Science Foundation of China (Grant No. 41825018, Grant No. 41574089 and Grant No. U20B2014), and the Second Tibetan Plateau Scientific Expedition and Research Program (STEP) under grant of No. 2019QZKK0904). We thank two reviewers for their critical and helpful suggestions and comments.

Open Access This article is licensed under a Creative Commons Attribution 4.0 International License, which permits use, sharing, adaptation, distribution and reproduction in any medium or format, as long as you give appropriate credit to the original author(s) and the source, provide a link to the Creative Commons licence, and indicate if changes were made. The images or other third party material in this article are included in the article's Creative Commons licence, unless indicated otherwise in a credit line to the material. If material is not included in the article's Creative Commons licence and your intended use is not permitted by statutory regulation or exceeds the permitted use, you will need to obtain permission directly from the copyright holder. To view a copy of this licence, visit <http://creativecommons.org/licenses/by/4.0/>.

Publisher's Note Springer Nature remains neutral with regard to jurisdictional claims in published maps and institutional affiliations.

REFERENCES

Chen, Z. A., Lin, B. H., Bai, W. M., et al. (2011). A study on the influence of the 2008 Wenchuan earthquake on the stability of

- the Qinghai-Tibet Plateau tectonic block system. *Tectonophysics*, 510, 94–103.
- Craig, C. H., & McKenzie, D. (1986). The existence of a thin low-viscosity layer beneath the lithosphere. *Earth and Planetary Science Letters*, 78, 420–426.
- Crampin, S. (2011). A second opinion on “Operational earthquake forecasting: some thoughts on why and how”, by Thomas H. Jordan and Lucile M. Jones. *Seismological Research Letters*, 82(2), 227–230.
- Crampin, S. (2012). Misunderstandings in comments and replies about the ICEF Report.
- Crampin, S., & Gao, Y. (2014). Two species of microcracks. *Applied Geophysics*, 11(1), 1–8.
- Crampin, S., & Gao, Y. (2018). Evidence supporting new geophysics. *Earth and Planetary Physics*, 2, 173–188.
- Ghahremani, F. (1980). Effect of grain boundary sliding on steady creep of polycrystals. *International Journal of Solids Structures*, 16, 847–862.
- Hansen, L. N., Zimmerman, M. E., & Kohlstedt, D. L. (2011). Grain boundary sliding in San Carlos olivine: Flow law parameters and crystallographic-preferred orientation. *Journal of Geophysical Research*, 116, B08201.
- Hirth, G., & Kohlstedt, D. L. (1995). Experimental constraints on the dynamics of the partially molten upper mantle: 2. Deformation in the dislocation creep regime. *Journal of Geophysical Research*, 100, 15441–15449.
- Hirth, G., & Kohlstedt, D. L. (2003). Rheology of the mantle wedge. In J. Eiler (Ed.), *Inside the subduction factory*. *Geophys. Monogr. Ser.* (Vol. 138, pp. 83–105).
- Jordan, T. H., & Jones, L. M. (2011). Reply to ‘A second opinion on “Operational earthquake forecasting: some thoughts on why and how”, by Thomas H. Jordan and Lucile M. Jones’, by Stuart Crampin. *Seismological Research Letters*, 82(2), 231–232.
- Karato, S. (2008). *Deformation of earth materials*. Cambridge University Press.
- Karato, S., Paterson, M., & Fitzgerald, J. (1986). Rheology of synthetic olivine aggregates: Influence of grain size and water. *Journal of Geophysical Research*, 91, 8151–8176.
- Peric, D., & Owen, D. R. J. (1992). Computational model for 3-D contact problems with friction based on the penalty method. *International Journal for Numerical Methods in Engineering*, 35, 1289–1309.
- Précigout, J., Gueydan, F., Gapais, D., Garrido, C., & Essaifi, A. (2007). Strain localisation in the subcontinental mantle—A ductile alternative to the brittle mantle. *Tectonophysics*, 445(3–4), 318–336.
- Warren, J. M., & Hirth, G. (2006). Grain size sensitive deformation mechanism in naturally deformed peridotites. *Earth and Planetary Science Letters*, 248(1–2), 438–450.
- Yang, S., Zhang, J., & Huang, Q. (2004). Analysis on creep compliance of cracked rock. *Chinese Journal of Rock Mechanics and Engineering*, 23(9), 1419–1423.
- Zienkiewicz, O. C., Taylor, R. L., & Zhu, J. Z. (2005). *The finite element method: its basis and fundamentals* (6th ed.). Singapore: Elsevier Pte Ltd.